A systematic study of embedded atom EXAFS: the (2 × 1)O/Cu(110) reconstruction as an ideal prototype system

2003 J. Phys.: Condens. Matter 15 5197

(http://iopscience.iop.org/0953-8984/15/30/302)

INSTITUTE OF PHYSICS PUBLISHING JOURNAL OF PHYSICS: CONDENSED MATTER

J. Phys.: Condens. Matter **15** (2003) 5197–5206 PII: S0953-8984(03)61047-7

A systematic study of embedded atom EXAFS: the (2 × 1)O/Cu(110) reconstruction as an ideal prototype system

H Wende[1,4,5], Ch Litwinski[2], A Scherz[2], T Gleitsmann[2], Z Li[2,6], C Sorg[2], K Baberschke[2], A Ankudinov[1], J J Rehr[1] and Ch Jung[3]

[1] Department of Physics, Box 351560, University of Washington, Seattle, WA 98195, USA
[2] Institut für Experimentalphysik, Freie Universität Berlin, Arnimallee 14, D-14195 Berlin-Dahlem, Germany
[3] BESSY GmbH, Albert-Einstein-Straße 15, D-12489 Berlin-Adlershof, Germany

E-mail: babgroup@physik.fu-berlin.de

Received 12 March 2003
Published 18 July 2003
Online at stacks.iop.org/JPhysCM/15/5197

Abstract

A systematic analysis of the embedded atom EXAFS (AXAFS) effect is presented. This effect is explained by the backscattering of the photoelectron at interstitial charge densities. The reconstructed (2 × 1)O/Cu(110) system is an ideal prototype system in which to study the angular dependence of the AXAFS because oxygen–copper rows are formed resulting in a C_2 symmetry. The scattering potential is non-spherical because of the high directionality of the O–Cu bonds. The high signal-to-noise ratio of the experimental data enables us to clearly identify the AXAFS contribution. Here we present the definite angular dependence of the experimental AXAFS for the first time, giving a unique opportunity to measure the anisotropy of the local embedded atom potential. The angular dependence demonstrates that the AXAFS effect cannot be mimicked by multi-electron excitations or experimental artifacts for this system. We compare our experiments to theoretical calculations within the muffin-tin approximation and show that future full-potential calculations are needed to model the angular dependence determined.

1. Introduction

This work provides further insight into the so-called atomic EXAFS (AXAFS) effect by investigating the angular dependence of the x-ray absorption coefficient for a strongly

[4] Author to whom any correspondence should be addressed.
[5] Permanent address: Institut für Experimentalphysik, Freie Universität Berlin, Arnimallee 14, D-14195 Berlin-Dahlem, Germany.
[6] Permanent address: Chemistry Department, University of Georgia, Athens, GA 30602, USA.

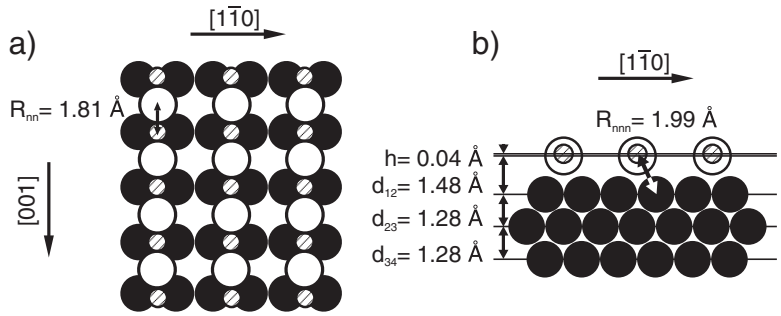

Figure 1. A schematic representation of the adsorption geometry for the (2 × 1)O/Cu(110) system in (a) top view and (b) side view as determined from this work. Small shaded circles: oxygen atoms; large open circles: Cu atoms of the first layer; full circles: Cu atoms of the second and following layers.

anisotropic surface system. While the regular EXAFS stems from the backscattering of the photoelectron at neighbouring atoms, the AXAFS contribution is assigned to the scattering at the charge densities placed between the atoms. Therefore, the AXAFS contribution to the entire fine structure of the x-ray absorption coefficient should be highly directional for systems with strong anisotropic bonding. This is the case for the reconstructed (2 × 1)O/Cu(110) surface system discussed here. There is general agreement that the O atoms are located in a long-bridge position along the [001] direction (see figure 1) forming O–Cu rows on the surface [1–10]. This C_2 symmetry results in a non-spherical scattering potential for the photoelectron. Therefore, a definite angular dependence of the AXAFS features is expected and reported here for the first time. Obviously, the O–Cu bond in the surface plane is highly directional. There are two different types of bond between the oxygen atoms and the first two Cu layers: the first bonding is between the O atoms (being located nearly in the surface plane) and the two Cu atoms of the first layer; the second bond is to the second layer. This local structure makes the (2 × 1)O/Cu(110) surface an ideal system in which to study the angular dependence of the atomic EXAFS contribution which is presented in this work. Therefore, temperature-dependent surface EXAFS (SEXAFS) measurements at the oxygen K edge are carried out for various polar and azimuthal orientations.

The presence of the controversial AXAFS effect (see e.g. [11–19]) was definitively observed for the low-Z elements nitrogen and oxygen for the (2 × 3)N/Cu(110) and ($\sqrt{2} \times 2\sqrt{2}$)R45°O/Cu(100) systems [20–23]. However, the lack of attention to the AXAFS effect over the years was partly due to the non-availability of high-quality EXAFS data. These data can nowadays be achieved at the new third-generation synchrotron sources where the gap of the undulator is scanned parallel to the monochromator. Light adsorbates on metal surfaces are established as model systems for this kind of investigation since no multi-electron excitations (MEEs) can mimic the long-range oscillatory fine structure in the x-ray absorption coefficient [21, 22] as can be the case for heavier atoms [13, 14, 18, 19]. Since the structural results presented in this work agree with the ones reported in the literature, the main focus of the present work is on the detailed analysis of the AXAFS contribution. The paper is structured as follows. We start with the description of the experimental details in section 2. In section 3 the experimental results are presented. Finally in section 4 the experimental results for the AXAFS are compared to *ab initio* calculations.

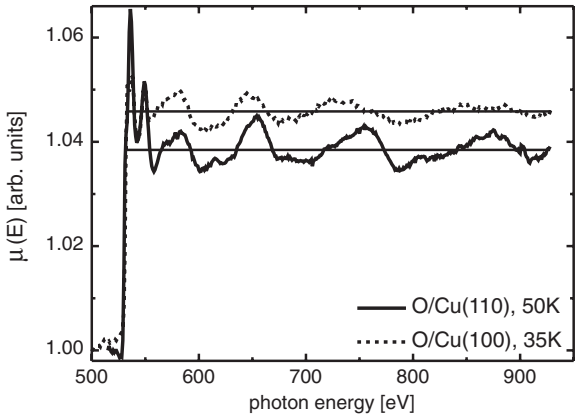

Figure 2. The x-ray absorption coefficient $\mu(E)$ at the O K edge of $(\sqrt{2} \times 2\sqrt{2})$R45°O/Cu(100) (dashed curve) [22] and (2×1)O/Cu(110) (solid curve). The spectra were divided by their spline functions.

2. Experimental details

To measure the azimuthal angular dependence, two Cu(110) single crystals from the same rod and of identical quality were mounted in the UHV chamber—one crystal rotated azimuthally by 90° with respect to the other one. The crystals were cleaned by successive cycles of argon-ion bombardment and annealing to 850 K. The surface was characterized by means of Auger electron spectroscopy and low-energy electron diffraction (LEED). The base pressure was $<3 \times 10^{-10}$ mbar. It is well known that chemisorption of oxygen on a Cu(110) surface leads to an adsorbate-induced missing row reconstruction. This reconstructed state was achieved after dosing 12 L of O_2 at room temperature and annealing to 400 K after dosage. With this procedure the saturation coverage of 0.5 ML was achieved, which was controlled by investigating the signal-to-background ratio (edge jump) versus the oxygen dosage. The experiments were performed at BESSY II in Berlin. We used the U-41 beamline with a collimated plane-grating monochromator (PGM) and a refocusing unit [24]. For the first time the so-called gap-scan technique was used over an energy range of $\Delta E = 430$ eV (see figure 2). Therefore, the high photon flux provided by the undulator set-up was combined with the feasibility of scanning the energy in an extended range [25, 26]. Hence, highly reliable SEXAFS data were measured which allowed a systematic investigation of the small AXAFS contribution. The SEXAFS data were taken at the O K edge with the quasi-total electron yield at a polar angle of $\alpha = 90°$ (normal x-ray incidence; E-vector parallel to surface) and $\alpha = 20°$ (grazing x-ray incidence) in both azimuths ([100] and $[1\bar{1}0]$).

3. Experimental results

In figure 2 the x-ray absorption coefficients $\mu(E)$ at the oxygen K edge are presented for the reconstructed systems (2×1)O/Cu(110) (this work) and $(\sqrt{2} \times 2\sqrt{2})$R45°O/Cu(100) [22]. The oscillatory fine structures are related because of the very similar nearest-neighbour distances (O/Cu(110): $R_{nn} = 1.81$ Å, O/Cu(100): $R_{nn} = 1.83$ Å). But for the O/Cu(110) system the amplitude of the oscillation is larger. This is due to the fact that the effective coordination number is higher for O/Cu(110) because for O/Cu(100) two domains of the reconstructed surface are probed which are rotated by 90°. The presence of the domains for

Table 1. Bond lengths and Einstein temperatures for the nearest- and the next-nearest-neighbour bonds.

	Nearest neighbour R_{nn}	Next-nearest neighbour R_{nnn}
Bond length R (Å)	1.81 ± 0.03	1.99 ± 0.03
Einstein temperature θ_E (K)	420 ± 40	380 ± 40

O/Cu(100) is also why an azimuthal angular dependence was not investigated in an earlier work [22]. The SEXAFS oscillations are extracted with stiff polynomial spline functions from the x-ray absorption coefficient $\mu(E)$ (which is divided by the spline function in figure 2 for clearer representation). Because of the higher intensity of the SEXAFS oscillations for O/Cu(110) the AXAFS feature can be detected even more reliably. It turns out that the AXAFS interferes destructively with the nearest-neighbour scattering contribution. This results in a reduction of the SEXAFS wiggle at about 680 eV which can be detected even by eye in both spectra.

The detailed analysis of the SEXAFS wiggles is carried out in k-space, as presented in the left-hand side of figure 3. The temperature-dependent data (50, 300 K) for the various polar and azimuthal orientations of the crystals are shown. The damping of the SEXAFS signals at 300 K is due to the larger dynamic disorder described by the mean square relative displacement (MSRD) $\sigma^2(T)$ which enters into the EXAFS Debye–Waller factor: $\exp[-2\sigma^2(T)k^2]$. From the temperature dependence of $\sigma_i^2(T)$ for every bond i, an Einstein temperature $\theta_{E,i}$ can be calculated that characterizes the bonding strength of every individual bond i [27]. The right-hand side of figure 3 shows the Fourier transforms of the data. As discussed above, the SEXAFS is mainly determined by the two bonds of the oxygen atoms to the Cu atoms as discussed above (R_{nn} and R_{nnn}). At normal incidence with the E-vector parallel to the O–Cu rows ($\vec{E} \parallel [001]$) the nearest-neighbour bond R_{nn} is probed (figures 3(a), (b)), whereas at grazing and at normal x-ray incidence with the E-vector perpendicular to the O–Cu rows ($\vec{E} \perp [001]$) the next-nearest-neighbour bond R_{nnn} of the O atoms to the second layer is analysed (figures 3(c)–(f)). That two different bonds are indeed probed can be seen by looking at the different phases of the SEXAFS oscillations in the k-space (figure 3, left) for (a), (b) compared to (c)–(f). Correspondingly, the main peak position in the Fourier transform (figure 3, right) is shifted to larger distances for (c)–(f) as indicated by the right-hand vertical lines. The reason for the larger intensity of the main peak in the Fourier transforms in (c), (d) compared to (e), (f) is due to the larger effective coordination number $N_i^* = 3\sum_j(\vec{\epsilon}\cdot\vec{r}_{i,j})^2$ for this measuring geometry. Here, $\vec{\epsilon}$ is the unit vector in the direction of the electric field and $\vec{r}_{i,j}$ is the unit vector in the direction of the bond, where j refers to all the backscattering atoms within a backscattering shell i. So, N_i^* is basically the sum over all the projections of the bonding directions $\vec{r}_{i,j}$ to the electric field vector $\vec{\epsilon}$. Fitting the main contributions in the Fourier transforms using FEFFIT [28] with a theoretical standard calculated with FEFF8.2 [29], the bond lengths and the corresponding Einstein temperatures $\theta_{E,i}$ can be determined, as given in table 1. From these results the structure given in figure 1 is concluded. The height of $h = 0.04$ Å of the oxygen atoms above the plane formed by the first Cu layer was determined by optimizing the intensity of the forward-focusing peak located at about 3.2 Å in figure 3(a) (right) using the FEFF8.2 code [26]. The next-nearest-neighbour length of bonds of the O atoms to the second Cu layer is consistent with a layer expansion of 0.20 Å of the first layer (see d_{12} and d_{23} in figure 1). Similar expansions were found in various other structural investigations of this system [9, 30–32]. The slightly larger Einstein temperature of the nearest-neighbour bond (see table 1) indicates that this bond is a little stiffer compared the next-nearest-neighbour one.

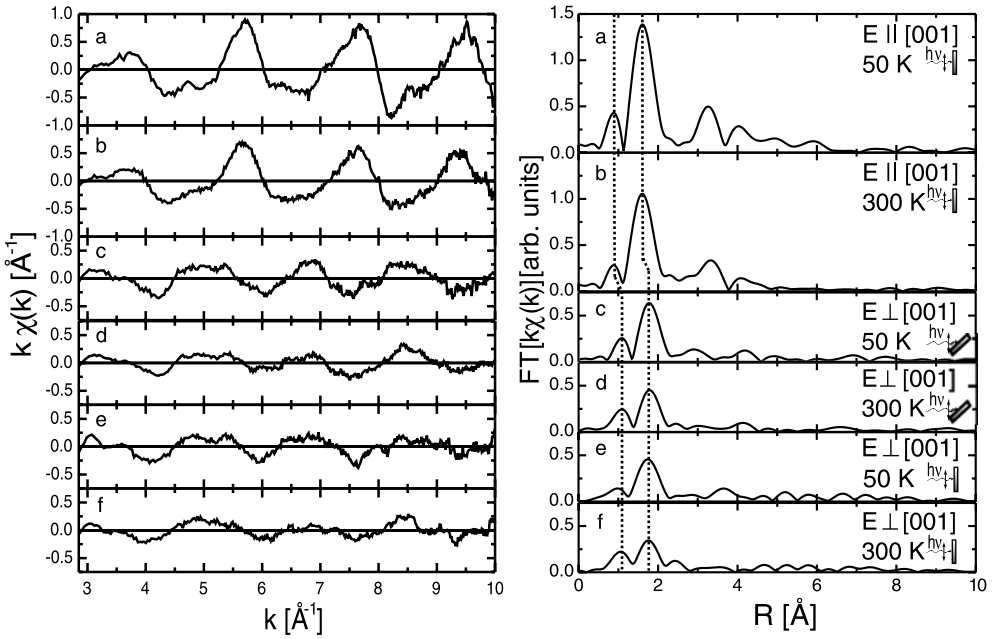

Figure 3. SEXAFS oscillations $k\chi(k)$ (left) and the corresponding Fourier transforms $|FT[k\chi(k)]|$ (right) for (2×1)O/Cu(110). The AXAFS and nearest-neighbour contributions are marked with dotted vertical lines.

But this anisotropy is small compared to those of other reconstructed systems (see e.g. [27]) demonstrating that the strengths of the bonding of the O atoms to the first and the second Cu layers for the present system is nearly isotropic, although the bond lengths are quite different (see table 1).

Now we turn to the investigation of the peak located at about half of the nearest-neighbour distance (Fourier transforms (a), (b) in figure 3) or at half of the next-nearest-neighbour distance (Fourier transforms (c)–(f) in figure 3). These contributions marked by the left vertical lines are assigned to the AXAFS contribution. Obviously these contributions shift systematically according to the bond which is probed. This demonstrates that these structures located at about 0.9 Å (AXAFS nearest neighbour) and 1.1 Å (AXAFS next-nearest neighbour) cannot be artifacts due to possible MEEs as discussed by Filipponi *et al* [14, 15]. This is because MEEs lead to structures at a fixed energy in the x-ray absorption coefficient $\mu(E)$. Therefore, features that originate from MEEs would show up at the same distance R in the Fourier transform, independently of the measuring geometry. The same argument is true for experimental artifacts which could be due to improper normalization of the data. Hence, the dependence of the AXAFS peak position on the bond being probed is a strong indication that this feature does indeed stem from the scattering at interstitial charges between the absorbing and the backscattering atom. For a more detailed investigation of the anisotropy of the AXAFS, the Fourier transforms of the SEXAFS oscillations with the E-vector along the O–Cu rows ($\vec{E} \parallel [001]$) and perpendicular to the O–Cu rows ($\vec{E} \perp [001]$) are directly compared in figure 4 (left). The AXAFS peak A shifts to larger distances A′ together with the position of the main peak (nearest neighbour: B; next-nearest neighbour B′). In order to analyse the phases of the AXAFS the Fourier backtransforms of the peaks marked A and A′ are presented in figure 4 (right). Interestingly, the AXAFS oscillation of the nearest-neighbour bond (solid curve)

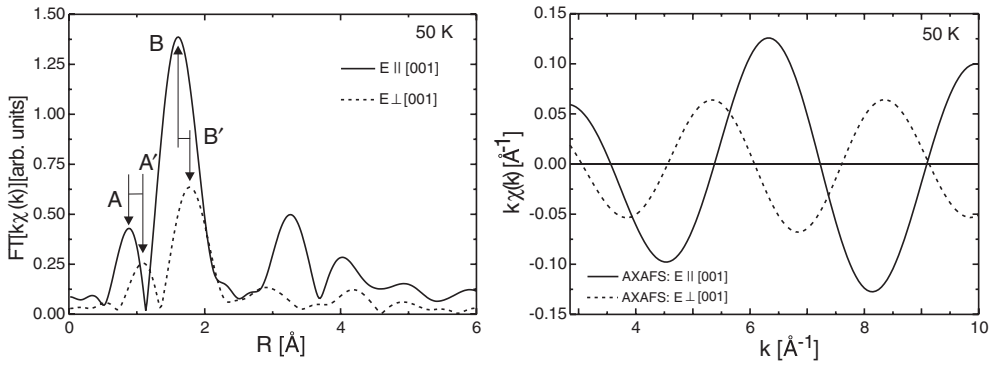

Figure 4. Left: direct comparison of the Fourier transformed SEXAFS data with the E-vector along the O–Cu bond ($\vec{E} \parallel [001]$, normal x-ray incidence) and perpendicular to that direction ($\vec{E} \parallel [1\bar{1}0]$, grazing x-ray incidence). Right: the Fourier backtransform of the AXAFS contributions labelled A and A′ in the left figure.

exhibits a maximum around $k \approx 6.3$ Å^{-1} whereas a minimum is determined for the regular SEXAFS oscillations at this k-value (figure 3(a) (left)). This results in a destructive interference of the two contributions leading to a dip in the enveloping amplitude of the complete SEXAFS as can be detected even by inspection by eye in figure 3(a) (left). This is also found for the next-nearest-neighbour bond. The AXAFS oscillation exhibits a minimum at $k \approx 6.8$ Å^{-1} (dashed curve in figure 4 (right)) whereas a maximum is found for the regular SEXAFS oscillations (figure 3(c) (left)).

The same trend can also be seen when comparing the SEXAFS oscillations of the present (2×1)O/Cu(110) system to the $(\sqrt{2} \times 2\sqrt{2})$R45°O/Cu(100) system investigated earlier [22] as presented in figure 5 (left). As discussed above, similar bondings are probed for the two cases and therefore a similar AXAFS contribution is expected. Indeed, a dip in the enveloping amplitude of the SEXAFS oscillations can be detected around $k \approx 6$ Å^{-1}. Looking at the Fourier transform of these oscillations as given in figure 5 (right), obviously the AXAFS (marked) is present for both cases. For O/Cu(110) the AXAFS contribution is about 30% of the main SEXAFS contribution, whereas it is about 50% for O/Cu(100). This relatively larger—by a factor of 1.6—AXAFS for O/Cu(100) compared to O/Cu(110) might be related to the different local geometries for the two cases: for O/Cu(100) the oxygen atoms are surrounded by three Cu atoms in the first layer, whereas only two Cu atoms enclose the oxygen atom for O/Cu(110) in the first layer. Furthermore, two structural domains of the reconstructed surface are probed for the O/Cu(100) systems which are rotated by 90°. This could result in a different localization of the interstitial charges leading to the effect discussed above. Interestingly, the AXAFS contributions exhibit about the same intensity on an absolute scale, which might indicate that the AXAFS intensity is basically determined by the nature of the bonding of oxygen to copper itself. This is also supported by the fact that the AXAFS peaks exhibit the same widths in the two cases. The similar shapes of the AXAFS peaks reveal that they cannot be due to an experimental artifact related to the beamline used, because the SEXAFS data were recorded at different synchrotron radiation facilities, namely BESSY II (O/Cu(110)) and BESSY I (O/Cu(100)).

4. Discussion

In order to investigate the AXAFS for this system in more detail we compare the experimental results to *ab initio* calculations using the FEFF8.2 code [29] based on spherical potentials

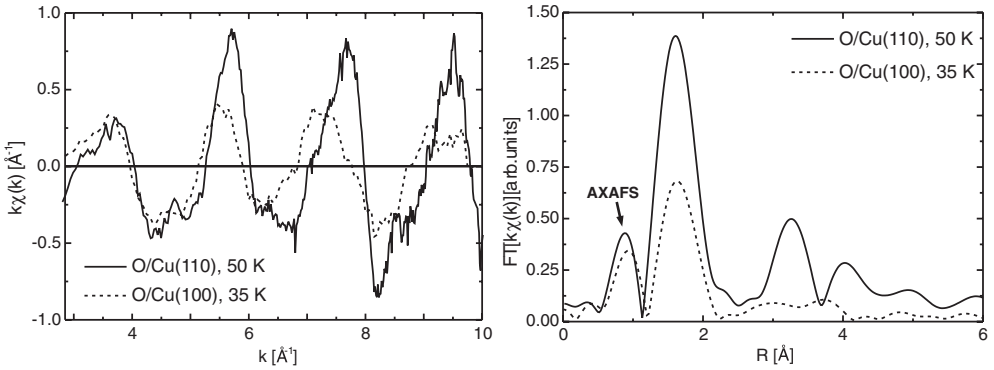

Figure 5. Left: direct comparison of the SEXAFS oscillations $k\chi(k)$ of the systems (2×1)O/Cu(110) (solid curve) and $\sqrt{2} \times 2\sqrt{2}$)R45°O/Cu(100) (dashed curve) for normal x-ray incidence (with the E-vector along the O–Cu bond in the surface plane for the O/Cu(110) system ($\vec{E} \parallel [001]$)). Right: Fourier transformed SEXAFS data. The AXAFS contribution is labelled.

(muffin-tin approximation). The scattering of the photoelectron at interstitial charge densities results in an oscillatory fine structure $\chi_e(E)$ of the atomic x-ray absorption coefficient $\mu_0(E)$ of the embedded atom:

$$\mu_0(E) = \mu_{0,\text{free}}(E)[1 + \chi_e(E)]. \tag{1}$$

Here, $\mu_{0,\text{free}}(E)$ refers to the smooth atomic x-ray absorption coefficient of the free atom. Therefore, the total x-ray absorption coefficient $\mu(E)$ becomes

$$\mu(E) = \mu_{0,\text{free}}(E)[1 + \chi_e(E)][1 + \chi(E)]. \tag{2}$$

In this representation of the total x-ray absorption coefficient the scattering of the photoelectron at the interstitial charges is separated from the scattering at neighbouring atoms. As suggested by Rehr and co-workers the AXAFS oscillatory fine structure $\chi_e(E)$ can be described in the muffin-tin approximation by [12]

$$\chi_e(E) = -\frac{1}{kR_{\text{MT}}^2}|f_e| \sin(2kR_{\text{MT}} + 2\delta_1^a + \phi_e). \tag{3}$$

Here, R_{MT} is the muffin-tin radius, $f_e = |f_e|e^{i\phi_e}$ is an effective curved-wave scattering amplitude of the interstitial charge density and δ_1^a is the central-atom phase shift. Looking at the AXAFS intensity relative to the nearest-neighbour contribution in the Fourier transform in figure 4, the AXAFS is about 30% of the main contribution. However, to determine the relative intensities of the effective scattering amplitudes for the interstitial charge $|f_e|$ and the effective backscattering amplitude of the nearest-neighbour $|f_{nn}|$, the relative intensities seen in the Fourier transform have to be rescaled by $1/R^2$. Since the AXAFS contribution is located approximately at half the nearest-neighbour distance, the ratio is $|f_e|/|f_{nn}| \approx 8\%$. Interestingly, in a simplified atomic picture one can assume that each bond consists of two electrons (f_e) and each of the nearest-neighbour Cu atoms (f_{nn}) has 27 ($3d^9$) or 28 ($3d^{10}$) electrons that scatter. Then the ratio becomes $|f_e|/|f_{nn}| = 2/28 \approx 7\%$. This value is in reasonable agreement with the experimentally determined ratio which supports the interpretation that AXAFS is due to the scattering from the bonding charges while the main EXAFS contribution originates from the charges localized at the nearest-neighbour atom. With the FEFF8.2 code we calculated the atomic x-ray absorption coefficient $\mu_0(E)$ as given in figure 6. An oscillatory fine structure can be seen in $\mu_0(E)$ which was extracted with a

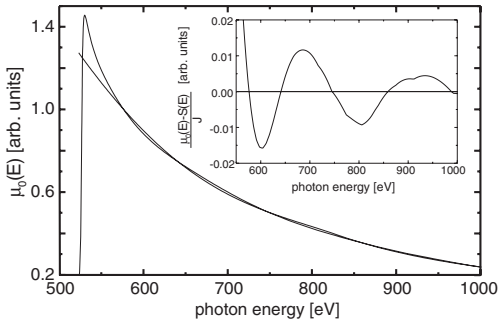

Figure 6. The atomic x-ray absorption coefficient $\mu_0(E)$ (thick curve) for the (2×1)O/Cu(110) system calculated using the FEFF8.2 code. The oscillatory fine structure which is extracted with a smooth polynomial spline function (thin curve) is presented in the inset.

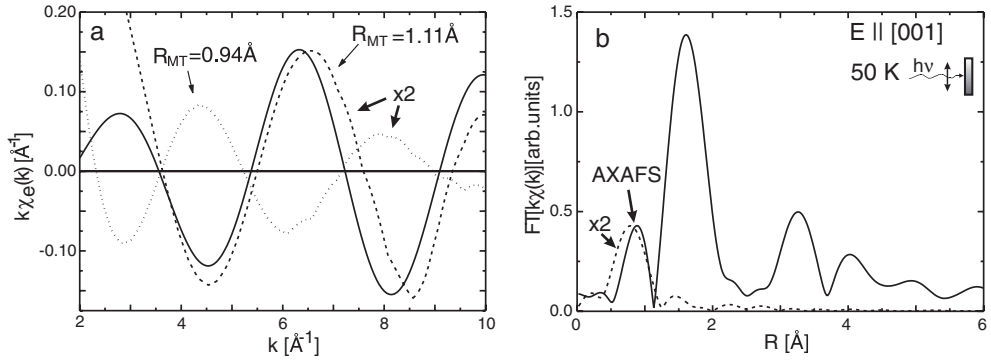

Figure 7. Left: calculated AXAFS χ_e for two muffin-tin radii ($R_{MT} = 0.94$ Å: dotted curve; $R_{MT} = 1.11$ Å: dashed curve) and the backtransformed experimental AXAFS contribution for O/Cu(110) (marked in figure 5) (solid curve). Right: the Fourier transform of the calculated AXAFS contribution ($R_{MT} = 1.11$ Å) (dashed curve) together with the Fourier transform of the complete experimental SEXAFS oscillations (solid curve).

stiff polynomial spline function. The result of this extraction is given in the inset of figure 6. The normalization of the data to a constant edge jump reveals that the calculated AXAFS intensity is about 2% of the edge jump. The calculated AXAFS oscillations are compared to the experimental result in figure 7. A muffin-tin radius of $R_{MT} = 0.94$ Å (dotted curve) was calculated by assuming charge neutrality. It turns out that the phase of the calculated AXAFS oscillations are off by about 180°. Since there is charge transfer from the Cu to the O atoms which is not automatically taken into account by the scattering potentials calculated with the program, the muffin-tin radius had to be enlarged to $R_{MT} = 1.11$ Å. This is because the muffin-tin radii are kept constant even in the self-consistent field approximation. It turns out that the phase is in reasonable agreement with the experimental data for the enlarged muffin-tin radius. Both calculations had to be multiplied by a factor of 2 to match the experimental intensity. This is probably due to the extended continuum picture used in the calculation that may underestimate the real jump of the potential at the surface. Unfortunately, the anisotropy of the AXAFS peak position in the Fourier cannot be calculated using the FEFF8.2 code in the spherical muffin-tin approximation. For this purpose a full-potential version of the code is needed which is under development now.

5. Conclusions

We present surface EXAFS data nearly free of noise measured at a third-generation synchrotron radiation facility. This enabled us to clearly identify the atomic EXAFS contribution in the spectra for the (2×1)O/Cu(110) surface system. It turns out that this system is an ideal prototype system for investigating the AXAFS since the O–Cu bonding is highly directional. Our angle-dependent study showed that the position of the AXAFS contribution in the Fourier transform reflects this anisotropy of the bond being probed. This gives a unique opportunity to measure the anisotropy of the local embedded atom potential for the first time. Since the x-ray absorption of the low-Z atom oxygen is investigated, no MEEs can mimic such a contribution. Therefore, the appearance of this feature can indeed be related to the scattering of the photoelectron at interstitial charge densities. The comparison to *ab initio* calculations showed that the position and the lineshape of the AXAFS contribution in the Fourier transform can be modelled theoretically. A future full-potential calculation is needed to model the experimentally determined angular dependence. This combined experimental and theoretical work may help in the study of the charge densities that are responsible for the bonding in, for instance, oxides in more detail in future works.

Acknowledgments

One of us (HW) wishes to thank the University of Washington and the Freie Universität Berlin for hospitality and support during his stay in Seattle, joining Professor Rehr's group. We thank the BESSY staff members for their technical assistance during the beamtime. This work is supported by BMBF (05 KS1 KEB4) and the DFG (Sfb 290).

References

[1] Döbler U, Baberschke K, Haase J and Puschmann A 1984 *Phys. Rev. Lett.* **52** 1437
[2] Döbler U, Baberschke K, Vvedensky D D and Pendry J B 1986 *Surf. Sci.* **178** 679
[3] Bader M, Puschmann A, Ocal C and Haase J 1986 *Phys. Rev. Lett.* **57** 3273
[4] Feidenhans'l R, Grey F, Johnson R L, Mochrie S G J, Bohr J and Nielsen M 1990 *Phys. Rev.* B **41** 5420
[5] Jensen F, Besenbacher F, Lægsgaard E and Stensgaard I 1990 *Phys. Rev.* B **41** 10233
[6] Coulman D J, Wintterlin J, Behm R J and Ertl G 1990 *Phys. Rev. Lett.* **64** 1761
[7] Besenbacher F, Jensen F, Lægsgaard E, Mortensen K and Stensgaard I 1991 *J. Vac. Sci. Technol.* B **9** 874
[8] Besenbacher F and Nørskov J K 1993 *Prog. Surf. Sci.* **44** 5
[9] Liu W, Wong C, Zeng H C and Mitchell K A R 1995 *Prog. Surf. Sci.* **50** 247
[10] Stahrenberg K, Richter Th, Esser N and Richter W 2000 *Phys. Rev.* B **61** 3043
[11] Holland B W, Pendry P, Pettifer R F and Bordas J 1978 *J. Phys. C: Solid State Phys.* **11** 633
[12] Rehr J J, Booth C H, Bridges F and Zabinsky S I 1994 *Phys. Rev.* B **49** 12347
[13] Di Cicco A and Filipponi A 1994 *Phys. Rev.* B **49** 12564
[14] Filipponi A and Di Cicco A 1995 *Phys. Rev.* A **52** 1072
[15] Filipponi A and Di Cicco A 1996 *Phys. Rev.* B **53** 9466
[16] Rehr J J, Zabinsky S I, Ankudinov A and Albers R C 1995 *Physica* B **208/209** 23
[17] Rehr J J, Booth C H, Bridges F and Zabinsky S I 1996 *Phys. Rev.* B **53** 9468
[18] Ramaker D E, Mojet B L, Koningsberger D C and O'Grady W E 1998 *J. Phys.: Condens. Matter* **10** 8753
[19] van Dorssen G E, Koningsberger D C and Ramaker D E 2002 *J. Phys.: Condens. Matter* **14** 13529
[20] Wende H, Arvanitis D, Tischer M, Chauvistré R, Henneken H, May F and Baberschke K 1997 *J. Physique* IV **7** C2 211
[21] Wende H, Srivastava P, Chauvistré R, May F and Baberschke K 1997 *J. Phys.: Condens. Matter* **9** L427
[22] Wende H and Baberschke K 1999 *J. Electron Spectrosc. Relat. Phenom.* **101–103** 821
[23] Wende H 1999 Extended x-ray absorption fine structure spectroscopy of surfaces and thin films: local structure, dynamic and magnetic properties *Doctoral Thesis* Freie Universität Berlin (Berlin: Verlag Dr Köster) (ISBN 3-89574-341-0)

[24] Jung Ch, Eggensten F, Hartlaub S, Follath R, Schmidt J S, Senf F, Weiss M R, Zeschke Th and Gudat W 2001 *Nucl. Instrum. Methods Phys. Res.* A **467/468** 485
[25] Follath R 2001 *Nucl. Instrum. Methods Phys. Res.* A **467/468** 418
[26] Litwinski Ch 2002 *Diploma Thesis* Freie Universität Berlin
[27] Wende H, Arvanitis D, Tischer M, Chauvistré R, Henneken H, May F and Baberschke K 1996 *Phys. Rev.* B **54** 5920
[28] Newville M, Ravel B, Haskel D, Rehr J J, Stern E A and Yacoby Y 1995 *Physica* B **208/209** 154
[29] Ankudinov A L, Ravel B, Rehr J J and Conradson S D 1998 *Phys. Rev.* B **58** 7565
[30] Parkin S R, Zeng H C, Zhou M Y and Mitchell K A R 1990 *Phys. Rev.* B **41** 5432
[31] van de Riet E, Smeets J B J, Fluit J M and Niehaus A 1990 *Surf. Sci.* **214** 111
[32] Dürr H, Fauster Th and Schneider R 1991 *Surf. Sci.* **244** 237